Neutralizing Aptamers Block S/RBD-ACE2 Interactions and Prevent Host Cell Infection

Xiaohui Liu, Yi-ling Wang, Jacky Wu, Jianjun Qi, Zihua Zeng, Quanyuan Wan, Zhenghu Chen,
Pragya Manandhar, Victoria S. Cavener, Nina R. Boyle, Xinping Fu, Eric Salazar,
Suresh V. Kuchipudi, Vivek Kapur, Xiaoliu Zhang, Michihisa Umetani, Mehmet Sen,
Richard C. Willson, Shu-hsia Chen, and Youli Zu*

Abstract: The receptor-binding domain (RBD) of the severe acute respiratory syndrome coronavirus 2 spike (S) protein plays a central role in mediating the first step of virus infection to cause disease: virus binding to angiotensin-converting enzyme 2 (ACE2) receptors on human host cells. Therefore, S/RBD is an ideal target for blocking and neutralization therapies to prevent and treat coronavirus disease 2019 (COVID-19). Using a target-based selection approach, we developed oligonucleotide aptamers containing a conserved sequence motif that specifically targets S/RBD. Synthetic aptamers had high binding affinity for S/RBD-coated virus mimics ($K_D \approx 7\,nM$) and also blocked interaction of S/RBD with ACE2 receptors ($IC_{50} \approx 5\,nM$). Importantly, aptamers were able to neutralize S protein-expressing viral particles and prevent host cell infection, suggesting a promising COVID-19 therapy strategy.

Introduction

Severe acute respiratory syndrome coronavirus 2 (SARS-CoV-2) is a novel coronavirus recently identified as the causative agent of coronavirus disease 2019 (COVID-19),[1] a respiratory disease exhibiting a wide range of clinical outcomes from mild disease to severe viral pneumonia and acute respiratory distress syndrome.[1b,2] Trimeric spike (S) proteins are densely glycosylated molecules on the surface of SARS-CoV-2.[3] The receptor-binding domain (RBD) of S protein mediates binding of the virus to angiotensin-converting enzyme 2 (ACE2) receptors on host cells, which is the first

step in cell entry and host infection.[3,4] Interaction of S/RBD with host cell ACE2 receptors involves dramatic conformational changes in S protein.[4a,5] Because of its critical function in host cell entry and virus dissemination, S/RBD is an ideal target for the development of vaccines,[6] neutralizing antibodies,[7] and blocking inhibitors.[4b,8] Aptamers are small-molecule ligands comprised of short, single-stranded oligonucleotides.[9] Target-specific aptamers can be developed from synthetic ssRNA/ssDNA libraries via Systematic Evolution of Ligands by Exponential (SELEX) enrichment.[10] Through their unique three-dimensional structures, aptamers specifically recognize and bind to a variety of targets with high affinity, similar to antigen-antibody interactions.[11] Recently, aptamers that target S/RBD with high affinity have been described.[12] However, the extent to which aptamers may effectively neutralize SARS-CoV-2 has not yet been explored.

Herein we report the development of ssDNA aptamers specific for viral S/RBD, which have capacity to neutralize SARS-CoV-2 virus and prevent host cell infection in vitro.

Results and Discussion

Characterization of aptamer sequences specific for viral S/RBD. To develop neutralizing aptamers against SARS-CoV-2, virus mimics were generated by conjugating purified His-tagged S/RBD proteins to Ni-Sepharose beads. SELEX was performed using S/RBD-coated virus mimics as targets

---

[*] Dr. X. Liu, Dr. J. Qi, Dr. Z. Zeng, Dr. Q. Wan, Dr. Z. Chen,
Dr. E. Salazar, Dr. Y. Zu
Department of Pathology and Genomic Medicine
Houston Methodist Hospital
Houston, TX 77030 (USA)
E-mail: yzu@houstonmethodist.org

Dr. Y. L. Wang, Dr. S. X. Chen
Center for Immunotherapy Research
Houston Methodist Research Institute
Houston, TX 77030 (USA)

J. Wu, Dr. X. Fu, Dr. X. Zhang, Dr. M. Umetani
Department of Biology and Biochemistry and Center for Nuclear
Receptor and Cell Signalling, University of Houston
Houston, TX 77204 (USA)

Dr. P. Manandhar, Dr. M. Sen
Department of Biology and Biochemistry, University of Houston
Houston, TX 77204 (USA)

Dr. R. C. Willson
Chemical and Biomolecular Engineering, University of Houston
Houston, TX 77204 (USA)

Dr. V. S. Cavener, N. R. Boyle, Dr. S. V. Kuchipudi
Animal Diagnostic Laboratory, Dept. of Veterinary and Biomedical
Sciences, and Huck Institutes of Life Sciences
Pennsylvania State University
University Park, PA 16802 (USA)

Dr. V. Kapur
Dept. of Animal Science and Huck Institutes of Life Sciences
Pennsylvania State University
University Park, PA 16802 (USA)

Supporting information and the ORCID identification number(s) for
the author(s) of this article can be found under:
https://doi.org/10.1002/anie.202100345.

(Figure S1a) and an ssDNA library consisting of a 40-mer random core sequence and 18-mer constant arm sequences at both ends (Figure 1b).[13] Six rounds of combined enrichment and counter-selection steps were performed (Figure S1b). To monitor SELEX progression, aptamer pools derived from each SELEX round were PCR-amplified and the evolving capacity to bind virus mimics was quantified (Figure S1c–e). The final aptamer pool products were assessed by next-generation sequencing and the enrichment progression from SELEX rounds 4 to 6 (R4 to R6) was calculated (Table S1). Phylogenetic trees of aptamers were generated from the 50 most predominant sequences in the final aptamer pool (R6) and potential motif sequences in each cluster of aptamer trees were determined (Figure 1a). From over 100 000 sequencing reads, three distinct sequence motifs accounting for 90%, 3%, and 1% of the total were identified. All motifs were found within central core sequences without involvement of

constant arm sequences (Figure S2). For functional validation, two representative aptamer sequences from the Motif 1 cluster (aptamers-1 and -2) and one sequence from the Motif 2 cluster (aptamer-6) were selected and listed along with the ssDNA library (Figure 1b). Minimum free energy secondary structures were predicted for selected aptamer sequences (Figure 1c). Further analysis revealed that the core sequences of Motif 1-derived aptamers-1 and -2 had very similar secondary structures while the core sequence of Motif 2-derived aptamer-6 differed significantly from these two (Figure 1d).

Functional analysis of aptamers to bind S/RBD and spike proteins. For functional assessment, selected aptamer sequences were synthesized and labeled with a Cy3 fluorescent reporter at 5′ end. Individual synthetic aptamers were incubated with virus mimics at room temperature (RT) for 25 min and resultant binding was quantified by flow cytom-

Figure 1. Aptamer sequences specific for viral S/RBD. a) Aptamers were developed using a target-based enrichment process and final products were sequenced. The top 50 predominant aptamer sequences were selected from over 100 000 reads. Phylogenetic tree analysis identified three well-preserved sequence motifs. b) Aptamers-1 and -2 were derived from the Motif 1 sequence and aptamer-6 from the Motif 2 sequence. Sequences of the ssDNA library used for aptamer development are also shown. Blue arrows indicate 18-mer consistent arm sequences at both ends for primer annealing of PCR amplification. Red lettering indicates central cores composed of 40-mer specific sequences of the aptamers or random sequences in the Random ssDNA library. c) Minimum free energy secondary structures of aptamers-1, -2, and -6. d) Core sequence comparison confirms different secondary structures for aptamers derived from Motif 1 and 2 sequences.

etry. Motif 1-derived aptamers-1 and -2 targeted S/RBD-virus mimics with high affinities, $K_D = 6.05 \pm 2.05$ nM and 6.95 ± 1.10 nM, respectively (Figure 2a). Notably, Motif 2-derived aptamer-6 had a similar K_D value, 7.52 ± 3.20 nM, but significantly lower maximal binding capacity (B_{max}) about one third of aptamers-1 and -2. All aptamers also targeted S protein-coated virus mimics (Figure 2b) but did not bind to control His-tag beads (Figure 2c). To determine whether the aptamers targeted the same site/epitope on S/RBD, competition binding assays were performed using individual aptamer probes in the presence of equal amounts of unlabeled competitive aptamer sequences. Motif 1-derived aptamers-1 and -2 competed for binding sites on virus mimics. However, only small competitive effects were noted between these aptamers and Motif 2-derived aptamer-6, indicating that sequence motifs likely drive aptamer target specificity or B_{max} (Figure 2d). In addition, aptamers were tested under variable conditions to confirm biocompatibility. As functional oligonucleotides, aptamers depend on magnesium (Mg^{2+}) ions for target binding activity. Aptamer binding to virus mimics was

fully functional within the physiologic Mg^{2+} concentration range, 0.65–1.10 mmol L^{-1} (Figure 2e). Further, aptamers similarly targeted S/RBD at temperatures ranging from 4–37°C (Figure 2f), indicating that they can function both in vitro and in vivo. Moreover, aptamers did not react with mixed culture cells or blood cells (Figure S3a, S3b) and were stable in human serum at 37°C for 24 h (Figure S5), suitable for clinical use.

To determine the functional sequences of the aptamers, 40-mer core sequences containing consensus Motif 1 structures were synthesized (Figure 1d). Binding assays revealed that the core sequences had the same capacity to bind virus mimics as the full-length aptamers (Figure 2g). To characterize target binding kinetics, surface plasmon resonance (SPR) studies were performed with purified and immobilized SARS-CoV-2 S proteins. Aptamers-1 and -2 had similar association and dissociation constants (k_a and k_d) (Figure 2h). In contrast, aptamer-6 showed faster k_a and k_d kinetics although its K_D value was nearly identical to aptamers-1 and -2 (Figure 2i).
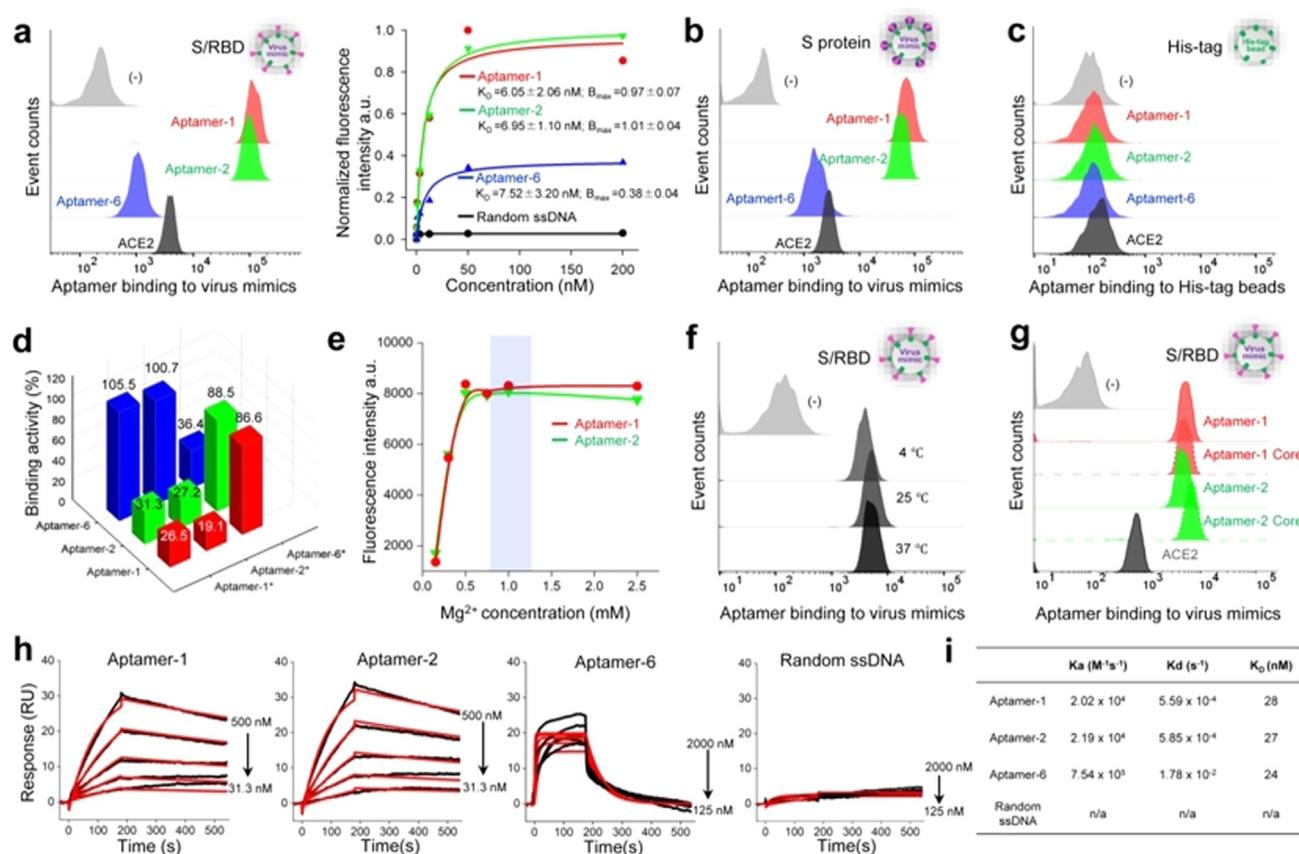
Figure 2. Functional characterization of aptamers. a) Binding assays of selected aptamers to S/RBD-virus mimics, which were used for target-based SELEX. Flow cytometry reveals that aptamers-1 and -2 containing Motif 1 sequences bound virus mimics with high capacity, while aptamer-6, containing the Motif 2 sequence, had significantly lower binding capacity. b) Aptamers targeted S protein-virus mimics with identical pattern. c) No aptamers reacted with control His-tag beads under the same experimental conditions. d) Competition assays demonstrated that aptamers-1 and -2 competed with each other for virus mimic binding but not with aptamer-6, suggesting that aptamers-1 and -2 target different S/RBD sites/epitopes than aptamer-6. e) Aptamers-1 and -2 were fully functional within the physiologic concentration range of magnesium. f) Aptamer-1 had the same target binding capacity at 4°C, 25°C, and 37°C. g) The central core sequences of aptamers-1 and -2 possessed full S/RBD binding capacity. h) Sensorgrams and kinetic binding parameters of aptamer binding to immobilized SARS-CoV-2 S proteins. Black lines: raw data; red lines: 1:1 Langmuir fitting. i) SPR studies reveal high binding capacity of aptamers-1 and -2 with very similar kinetics of association and dissociation constants (k_a and k_d, respectively). In contrast, aptamer-6 had faster k_a and k_d kinetics. Although aptamers showed significantly different k_a and k_d, they had similar K_D values ranging from 24–28 nM.

Aptamers block S/RBD-ACE2 interaction and neutralize viral particles. To effectively neutralize SARS-CoV-2, aptamers need not only to specifically target S/RBD but also block its interaction with ACE2 receptors. To determine the ability of the aptamers to block S/RBD-ACE2 interactions, enzyme-linked immunosorbent assays (ELISA) were performed. First, biotinylated S/RBD proteins were mixed with serial dilutions of aptamers and then added into microplates pre-coated with purified ACE2 receptor proteins to mimic the host cell surface (Figure 3a). After incubation at RT for 30 min, resultant S/RBD-ACE2 binding was quantified by measuring reaction color intensity with a microplate reader. Aptamers-1 and -2 blocked S/RBD binding to ACE2 in a dose-dependent manner. In contrast, aptamer-6 did not affect S/RBD-ACE2 interactions. Similar findings were observed in binding assays using microplates pre-coated with S/RBD or S protein to mimic virus surface (Figure 3b,c). Notably, aptamer-mediated blocking effects occurred at 4°C, 25°C, and 37°C (Figure S3c), indicating that aptamers are suitable for in vivo use. Next, HEK293T cells stably express-ing ACE2 (ACE-293T) were used as host cells in blocking assays. Biotinylated S/RBD proteins were mixed with serially diluted aptamers and then incubated with cultured ACE-293T host cells at RT for 1 h (Figure 3d). For reporting purposes, treated cells were stained with Cy3-labeled strep-tavidin and resultant changes in host cell binding of S/RBD were quantified by flow cytometry. Treatments with aptamers-1 and -2 blocked S/RBD protein binding to host cells with $IC_{50} = 5.2$ nM and 4.4 nM, respectively. Aptamer-6 had min-imal blocking effects and control random ssDNA sequences had no effect. Aptamer-induced blockage of S/RBD-host cell interaction was also confirmed by fluorescent microscopic examination of treated cells. To assess the ability of aptamers to target native S proteins, we generated pseudoviruses which are recombinant lentiviral particles expressing surface SARS-CoV-2 S proteins and carrying a firefly luciferase reporter gene. Serially diluted pseudovirus was pre-immobilized on microplates and then treated with biotinylated aptamers (Figure 3e). Biotinylated ACE2 receptor proteins were used as a positive control probe. Quantitative ELISA analysis
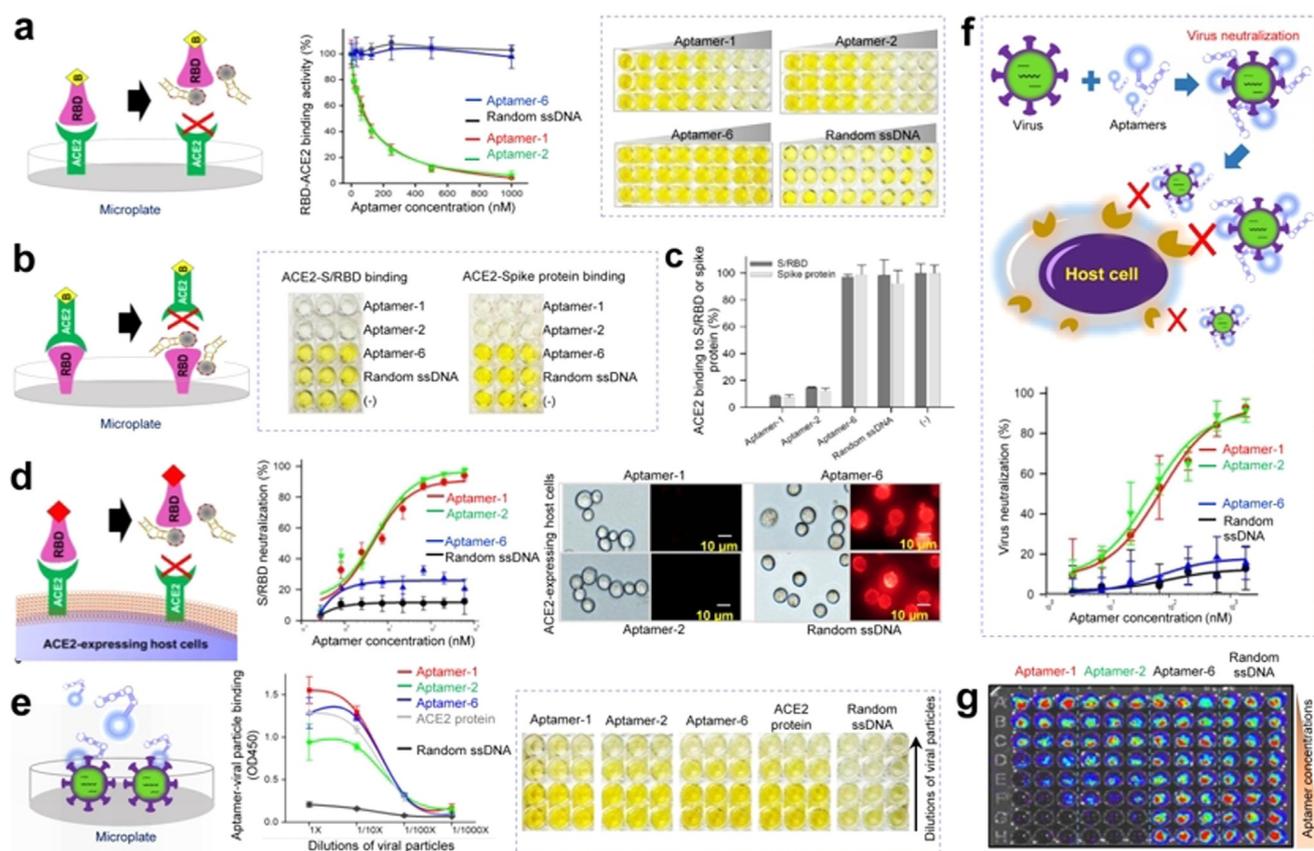
Figure 3. Aptamers block S/RBD-ACE2 interaction and neutralize viral particles to prevent host cell infection. a) Schematic depicting aptamer-mediated blockade of S/RBD-ACE2 interaction. ELISA reveals that aptamers-1 and -2 block S/RBD binding to ACE2 receptor proteins precoated on microplates (mimicking host cell surface). In contrast, aptamer-6 and random ssDNA sequences have no blocking effects under the same conditions. b) Aptamers-1 and -2 prevent ACE2 binding to S/RBD and c) S proteins precoated on microplates (mimicking virus surface). d) Flow cytometry and fluorescent microscopy demonstrate that aptamers-1 and -2 interrupt S/RBD binding to ACE2-expressing host cells. Aptamer-6 shows minimal blocking effects and random ssDNA sequences have no effect. e) Aptamers specifically target S protein-expressing viral particles in a virus dose-dependent manner, similar to the pattern observed with ACE2 protein. f) Virus neutralization assays. Aptamers-1 and -2 effectively neutralize viral particles and prevent host cell infection, while aptamer-6 and control random ssDNA sequences do not. g) Aptamer virus neutralization effects were also confirmed post-treatment using bioluminescent imaging of microplates, which contained intact host cells in the presence of luciferin for signal development.

demonstrated that aptamers bound viral particles in a virus dose-dependent manner, similar to results achieved with ACE2.

Finally, to interrogate aptamer therapeutic potential, virus neutralization assays were performed using a paired S protein-expressing viral particle and ACE-293T host cell system. Because the viral particles carry the luciferase reporter gene, viral infection results in intracellular expression of luciferase in host cells. Accordingly, the activity of cellular luciferase is proportional to viral infection intensity and the number of infected cells. ACE-293T host cells were pre-seeded into microplates overnight. Viral particles mixed with serial dilutions of aptamers were added to microplates containing host cells. After a short spinoculation and incubation at 37 °C for 2 h to allow virus infection, old medium was replaced with fresh and cells were further cultured at 37 °C for 72 h. To evaluate viral infection rates, treated host cells were lysed in microplates and cellular luciferase activity was evaluated using a Luciferin assay kit. Resultant signals were detected using a microplate luminometer. Quantitative analysis revealed that aptamers-1 and -2 neutralized viral particles and prevented host cell infection with neutralization $IC_{50} = 76.9$ nM and 53.0 nM, respectively (Figure 3 f). Aptamer-6 and random ssDNA sequences had little or no neutralization effects under the same experimental conditions. These findings were also confirmed by post-treatment bioluminescent imaging of microplates, which contained intact host cells in the presence of luciferin for signal development (Figure 3 g).

To assess clinical potential of the aptamers, we conducted a pilot study using the conventional microneutralization assay system composed of primary SARS-CoV-2 strain USA-WA1/2020 and host Vero E6 cells.[14] Figure S6 reveals that treatments of aptamers-1 and -2 resulted in virus neutralization and efficiently protected host cells from virus infection. In contract, control aptamer-6 and random ssDNA sequences had no effect on host cell infection by primary virus under the same condition. To understand whether our aptamers also neutralize other coronaviruses, additional studies are undergoing currently to determine binding specificity and affinity of the aptamers to SARS and MERS, as well as the variants of SARS-CoV-2. Resultant findings will be reported in near future separately.

For virus neutralization, aptamers need not only to specifically target S/RBD but also block its interaction with ACE2 receptors. Functional assays revealed that, although aptamer-6 possesses very similar K_D to aptamers-1 and -2 to bind S/RBD, it failed to block the S/RBD-ACE2 interaction. This failure may be due to its fast k_a and k_d kinetics that result in lower B_{max} to bind S/RBD and/or variation in targeting sites or epitopes on S/SRBD. For detection of SARS-CoV-2, our lab developed aptamers using S protein-coated virus mimics for target-based SELEX (Figure S4a, S4b). The selected S aptamers specifically targeted S protein with high binding affinity (Figure S4c) and also bound to S/RBD-virus mimics with similar pattern to those achieved by ACE2 protein control (Figure S4d). Notably, although S aptamers have the ability to bind to S/RBD, they failed to block the interaction of S/RBD with ACE2-expressing host cells (Figure S4e). A likely explanation for this is that the S/RBD site(s) targeted

by S aptamers is/are not involved in the S/RBD-ACE2 interaction. In addition, we have observed that 40-mer core sequences of aptamers-1 and -2 can neutralize S/RBD and prevent its binding to viral particles, indicating that failure to block S/RBD function is not due to the small size of aptamers (unpublished data). Therefore, future studies aiming to identify neutralizing aptamers against SARS-CoV-2 should evaluate binding kinetic features, B_{max}, and S/RBD targeting sites or epitopes.

To enhance the degree of effective virus neutralization, aptamer cocktails that allow targeting of multiple S/RBD epitopes may show promise. To this end, identification of additional aptamers containing different motif sequences specific for S/RBD with favorable binding kinetics and blocking capacity is required. Because of their synthetic oligonucleotide properties, multivalent aptamer nanostructures can be formulated through covalent or non-covalent methods. Such aptamer polymer nanostructures can simultaneously target multiple S/RBD molecules on individual viruses and, thus, may augment binding affinity to achieve higher virus neutralization efficacy.

Conclusion

In summary, this proof-of-concept study demonstrates that synthetic ssDNA aptamers can block S/RBD-ACE2 interactions, neutralize SARS-CoV-2 virus, and prevent host cell infection in vitro. The development of neutralizing aptamers provides a new promising therapeutic approach to treat COVID-19, in addition to neutralization antibodies and molecular blockers. To validate the clinical utility of neutralizing aptamers, our lab is pursuing preclinical studies with authentic SARS-CoV-2 virus and primary natural host cells is indispensable. Notably, while this submission was under review, a related study was published.[15]

Conflict of interest

The authors declare no conflict of interest.

[1] a) P. Zhou, X. L. Yang, X. G. Wang, B. Hu, L. Zhang, W. Zhang, H. R. Si, Y. Zhu, B. Li, C. L. Huang, H. D. Chen, J. Chen, Y. Luo, H. Guo, R. D. Jiang, M. Q. Liu, Y. Chen, X. R. Shen, X. Wang, X. S. Zheng, K. Zhao, Q. J. Chen, F. Deng, L. L. Liu, B. Yan, F. X. Zhan, Y. Y. Wang, G. F. Xiao, Z. L. Shi, *Nature* **2020**, *579*, 270–273; b) N. Zhu, D. Y. Zhang, W. L. Wang, X. W. Li, B. Yang, J. D. Song, X. Zhao, B. Y. Huang, W. F. Shi, R. J. Lu, P. H. Niu,

F. X. Zhan, X. J. Ma, D. Y. Wang, W. B. Xu, G. Z. Wu, G. G. F. Gao, W. J. Tan, *N. Engl. J. Med.* **2020**, *382*, 727 – 733; c) F. Wu, S. Zhao, B. Yu, Y. M. Chen, W. Wang, Z. G. Song, Y. Hu, Z. W. Tao, J. H. Tian, Y. Y. Pei, M. L. Yuan, Y. L. Zhang, F. H. Dai, Y. Liu, Q. M. Wang, J. J. Zheng, L. Xu, E. C. Holmes, Y. Z. Zhang, *Nature* **2020**, *579*, 265 – 269.

[2] a) C. L. Huang, Y. M. Wang, X. W. Li, L. L. Ren, J. P. Zhao, Y. Hu, L. Zhang, G. H. Fan, J. Y. Xu, X. Y. Gu, Z. S. Cheng, T. Yu, J. A. Xia, Y. Wei, W. J. Wu, X. L. Xie, W. Yin, H. Li, M. Liu, Y. Xiao, H. Gao, L. Guo, J. G. Xie, G. F. Wang, R. M. Jiang, Z. C. Gao, Q. Jin, J. W. Wang, B. Cao, *Lancet* **2020**, *395*, 497 – 506; b) E. S. Dong, H. R. Du, L. Gardner, *Lancet Infect. Dis.* **2020**, *20*, 533 – 534.

[3] A. C. Walls, Y. J. Park, M. A. Tortorici, A. Wall, A. T. McGuire, D. Veesler, *Cell* **2020**, *181*, 281 – 292.

[4] a) R. H. Yan, Y. Y. Zhang, Y. N. Li, L. Xia, Y. Y. Guo, Q. Zhou, *Science* **2020**, *367*, 1444 – 1448; b) M. Hoffmann, H. Kleine-Weber, S. Schroeder, N. Kruger, T. Herrler, S. Erichsen, T. S. Schiergens, G. Herrler, N. H. Wu, A. Nitsche, M. A. Muller, C. Drosten, S. Pohlmann, *Cell* **2020**, *181*, 271 – 280; c) J. Lan, J. W. Ge, J. F. Yu, S. S. Shan, H. Zhou, S. L. Fan, Q. Zhang, X. L. Shi, Q. S. Wang, L. Q. Zhang, X. Q. Wang, *Nature* **2020**, *581*, 215 – 220.

[5] a) D. Wrapp, N. S. Wang, K. S. Corbett, J. A. Goldsmith, C. L. Hsieh, O. Abiona, B. S. Graham, J. S. McLellan, *Science* **2020**, *367*, 1260 – 1263; b) A. C. Walls, X. L. Xiong, Y. J. Park, M. A. Tortorici, J. Snijder, J. Quispe, E. Cameroni, R. Gopal, M. Dai, A. Lanzavecchia, M. Zambon, F. A. Rey, D. Corti, D. Veesler, *Cell* **2019**, *176*, 1026 – 1039.

[6] a) J. Y. Yang, W. Wang, Z. M. Chen, S. Y. Lu, F. L. Yang, Z. F. Bi, L. L. Bao, F. Mo, X. Li, Y. Huang, W. Q. Hong, Y. Yang, Y. Zhao, F. Ye, S. Lin, W. Deng, H. Chen, H. Lei, Z. Q. Zhang, M. Luo, H. Gao, Y. Zheng, Y. Q. Gong, X. H. Jiang, Y. F. Xu, Q. Lv, D. Li, M. N. Wang, F. D. Li, S. Y. Wang, G. P. Wang, P. Yu, Y. J. Qu, L. Yang, H. X. Deng, A. P. Tong, J. Li, Z. L. Wang, J. L. Yang, G. B. Shen, Z. W. Zhao, Y. H. Li, J. W. Luo, H. Q. Liu, W. H. Yu, M. L. Yang, J. W. Xu, J. B. Wang, H. Y. Li, H. X. Wang, D. X. Kuang, P. P. Lin, Z. T. Hu, W. Guo, W. Cheng, Y. L. He, R. Song, C. Chen, Z. H. Xue, S. H. Yao, L. Chen, X. L. Ma, S. Y. Chen, M. L. Gou, W. J. Huang, Y. C. Wang, C. F. Fan, Z. X. Tian, M. Shi, F. S. Wang, L. Z. Dai, M. Wu, G. Li, G. Y. Wang, Y. Peng, Z. Y. Qian, C. H. Huang, J. Y. N. Lau, Z. L. Yang, Y. Q. Wei, X. B. Cen, X. Z. Peng, C. Qin, K. Zhang, G. W. Lu, X. W. Wei, *Nature* **2020**, *586*, 572 – 577; b) J. Y. Yu, L. H. Tostanoski, L. Peter, N. B. Mercado, K. McMahan, S. H. Mahrokhian, J. P. Nkolola, J. Y. Liu, Z. F. Li, A. Chandrashekar, D. R. Martinez, C. Loos, C. Atyeo, S. Fischinger, J. S. Burke, M. D. Slein, Y. Z. Chen, A. Zuiani, F. J. N. Lelis, M. Travers, S. Habibi, L. Pessaint, A. Van Ry, K. Blade, R. Brown, A. Cook, B. Finneyfrock, A. Dodson, E. Teow, J. Velasco, R. Zahn, F. Wegmann, E. A. Bondzie, G. Dagotto, M. S. Gebre, X. He, C. Jacob-Dolan, M. Kirilova, N. Kordana, Z. J. Lin, L. F. Maxfield, F. Nampanya, R. Nityanandam, J. D. Ventura, H. H. Wan, Y. F. Cai, B. Chen, A. G. Schmidt, D. R. Wesemann, R. S. Baric, G. Alter, H. Andersen, M. G. Lewis, D. H. Barouch, *Science* **2020**, *369*, 806 – 811; c) W. B. Tai, L. He, X. J. Zhang, J. Pu, D. Voronin, S. B. Jiang, Y. S. Zhou, L. Y. Du, *Cell. Mol. Immunol.* **2020**, *17*, 613 – 620.

[7] a) J. D. Huo, A. Le Bas, R. R. Ruza, H. M. E. Duyvesteyn, H. Mikolajek, T. Malinauskas, T. K. Tan, P. Rijal, M. Dumoux, P. N. Ward, J. S. Ren, D. M. Zhou, P. J. Harrison, M. Weckener, D. K. Clare, V. K. Vogirala, J. Radecke, L. Moynie, Y. G. Zhao, J. Gilbert-Jaramillo, M. L. Knight, J. A. Tree, K. R. Buttigieg, N. Coombes, M. J. Elmore, M. W. Carroll, L. Carrique, P. N. M. Shah, W. James, A. R. Townsend, D. I. Stuart, R. J. Owens, J. H. Naismith, *Nat. Struct. Mol. Biol.* **2020**, *27*, 846 – 854; b) L. H. Liu, P. F. Wang, M. S. Nair, J. Yu, M. Rapp, Q. Wang, Y. Luo, J. F. W.

Chan, V. Sahi, A. Figueroa, X. V. Guo, G. Cerutti, J. Bimela, J. Gorman, T. Q. Zhou, Z. W. Chen, K. Y. Yuen, P. D. Kwong, J. G. Sodroski, M. T. Yin, Z. Z. Sheng, Y. X. Huang, L. Shapiro, D. D. Ho, *Nature* **2020**, *584*, 450 – 456; c) X. Y. Chi, R. H. Yan, J. Zhang, G. Y. Zhang, Y. Y. Zhang, M. Hao, Z. Zhang, P. F. Fan, Y. Z. Dong, Y. L. Yang, Z. S. Chen, Y. Y. Guo, J. L. Zhang, Y. N. Li, X. H. Song, Y. Chen, L. Xia, L. Fu, L. H. Hou, J. J. Xu, C. M. Yu, J. M. Li, Q. Zhou, W. Chen, *Science* **2020**, *369*, 650 – 655.

[8] a) H. Su, F. Zhou, Z. Huang, X. Ma, K. Natarajan, M. Zhang, Y. Huang, H. Su, *Angew. Chem. Int. Ed.* **2021**, https:doi/full/10.1002/anie.202008835; *Angew. Chem.* **2021**, https:doi/full/10.1002/ange.202008835; b) O. V. de Oliveira, G. B. Rocha, A. S. Paluch, L. T. Costa, *J. Biomol. Struct. Dyn.* **2020**, https://doi.org/10.1080/07391102.2020.1772885; c) J. D. Huo, Y. G. Zhao, J. S. Ren, D. M. Zhou, H. M. E. Duyvesteyn, H. M. Ginn, L. Carrique, T. Malinauskas, R. R. Ruza, P. N. M. Shah, T. K. Tan, P. Rijal, N. Coombes, K. R. Bewley, J. A. Tree, J. Radecke, N. G. Paterson, P. Supasa, J. Mongkolsapaya, G. R. Screaton, M. Carroll, A. Townsend, E. E. Fry, R. J. Owens, D. I. Stuart, *Cell Host Microbe* **2020**, *28*, 497 – 497; d) M. D. Sacco, C. Ma, P. Lagarias, A. Gao, J. A. Townsend, X. Meng, P. Dube, X. Zhang, Y. Hu, N. Kitamura, B. Hurst, B. Tarbet, M. T. Marty, A. Kolocouris, Y. Xiang, Y. Chen, J. Wang, *Sci. Adv.* **2020**, *6*, eabc0751.

[9] D. L. Robertson, G. F. Joyce, *Nature* **1990**, *344*, 467 – 468.

[10] a) C. Tuerk, L. Gold, *Science* **1990**, *249*, 505 – 510; b) A. D. Ellington, J. W. Szostak, *Nature* **1990**, *346*, 818 – 822.

[11] a) L. Cerchia, C. L. Esposito, S. Camorani, A. Rienzo, L. Stasio, L. Insabato, A. Affuso, V. de Franciscis, *Mol. Ther.* **2012**, *20*, 2291 – 2303; b) P. H. L. Tran, D. X. Xiang, T. N. G. Nguyen, T. T. D. Tran, Q. Chen, W. Yin, Y. M. Zhang, L. X. Kong, A. Duan, K. S. Chen, M. M. Sun, Y. li, Y. C. Hou, Y. M. Zhu, Y. C. Ma, G. Q. Jiang, W. Duan, *Theranostics* **2020**, *10*, 3849 – 3866; c) D. Muharemagic, A. Zamay, S. M. Ghobadloo, L. Evgin, A. Savitskaya, J. C. Bell, M. V. Berezovski, *Mol. Ther. Nucl. Acids* **2014**, *3*, e167; d) W. G. He, M. A. Elizondo-Riojas, X. Li, G. L. R. Lokesh, A. Somasunderam, V. Thiviyanathan, D. E. Volk, R. H. Durland, J. Englehardt, C. N. Cavasotto, D. G. Gorenstein, *Biochemistry* **2012**, *51*, 9592 – 9592; e) J. H. Zhou, J. Rossi, *Nat. Rev. Drug Discovery* **2017**, *16*, 181 – 202; f) H. R. Culver, J. R. Clegg, N. A. Peppas, *Acc. Chem. Res.* **2017**, *50*, 170 – 178.

[12] a) Y. L. Song, J. Song, X. Y. Wei, M. J. Huang, M. Sun, L. Zhu, B. Q. Lin, H. C. Shen, Z. Zhu, C. Y. Yang, *Anal. Chem.* **2020**, *92*, 9895 – 9900; b) L. Y. Zhang, X. N. Fang, X. B. Liu, H. C. Ou, H. Y. Zhang, J. J. Wang, Q. Li, H. Y. Cheng, W. Y. Zhang, Z. F. Luo, *Chem. Commun.* **2020**, *56*, 10235 – 10238.

[13] K. Sefah, D. Shangguan, X. L. Xiong, M. B. O'Donoghue, W. H. Tan, *Nat. Protoc.* **2010**, *5*, 1169 – 1185.

[14] E. Salazar, S. V. Kuchipudi, P. A. Christensen, T. Eagar, X. Yi, P. Zhao, Z. Jin, S. W. Long, R. J. Olsen, J. Chen, B. Castillo, C. Leveque, D. Towers, J. Lavinder, J. Gollihar, J. Cardona, G. Ippolito, R. Nissly, I. Bird, D. Greenawalt, R. M. Rossi, A. Gontu, S. Srinivasan, I. Poojary, I. M. Cattadori, P. J. Hudson, N. M. Josleyn, L. Prugar, K. Huie, A. Herbert, D. W. Bernard, J. M. Dye, V. Kapur, J. M. Musser, *J. Clin. Invest.* **2020**, *130*, 6728 – 6738.

[15] M. Sun, S. Liu, X. Wei, S. Wan, M. Huang, T. Song, Y. Lu, X. Weng, Z. Lin, H. Chen, Y. Song, C. Yang, *Angew. Chem. Int. Ed.* **2021**, https://doi.org/10.1002/anie.202100225; *Angew. Chem.* **2021**, https://doi.org/10.1002/ange.202100225.